The European Large Area ISO Survey *

Seb Oliver & Francesca Pozzi
Astronomy Centre, Dept. of Physics & Astronomy, University of Sussex, Brighton, BN1 9QH, UK
Dipartimento di Astronomia, Università di Bologna, via Ranzani 1, ID40127 Bologna, Italy

Abstract. The European Large Area ISO Survey, ELAIS, was the largest Open Time survey on the Infrared Space Observatory, ISO. It was designed to explore obscured galaxies and hence quantify the recent star-formation history of the Universe. The final reanalysis of the data has been completed and a band-merged catalogue with associations across many wavelengths compiled and released the data to the global astronomical community (http://astro.imperial.ac.uk/Elais/). This paper summarizes some of the key results.

Keywords: infrared, galaxies, evolution, cosmology, observations

Abbreviations: KAP – Kluwer Academic Publishers; compuscript – Electronically submitted article

Received: 14 July 2004 **Revised:** 21 October 2004

1. The ELAIS Project

The European Large Area ISO Survey was the largest non-serendipitous project on ESA's Infrared Space Observatory (ISO, [1],[2]) using ISOCAM [3], [4] and ISOPHOT [5], [6]. The survey covered around 12 square degrees, with ISO data at 6.7, 15, 90 and 175μm. To reduce the effect of cosmic variance, ELAIS was split into 3 fields of comparable sizes, 2 in the north (N1, N2) and 1 in the south (S1), plus 6 smaller area. The aims of the project and a detailed description of the observations can be found in [7]. A Preliminary Analysis was undertaken to provide early scientific results and to provide follow-up source lists at 6.7 and 15μm [8], 90μm[9] – the 175μm data was processed by the FIRBACK consortium [10]. To extract the maximum information from the ISO data a very careful Final Analysis of the 15μm data [11], [12], and at 90μm[13] was undertaken. The infrared catalogues have also been cross-correlated with each other and associated with complementary optical, NIR and radio catalogues (including [14], [15], [16], [17], [18], [19]). The final ISO and Radio selected compilation comprises nearly 4000 sources with limiting flux densities at 6.7, 15, 90 and 175μm of $\sim$ 1.0, 0.7, 70 and 223 mJy [20], these "band-merged" catalogues have been made public (http://astro.imperial.ac.uk/Elais/).

* Based ¿ on observations with ISO, an ESA project ¿ with instruments funded by ESA Member States (especially ¿ the PI countries: France, Germany, the Netherlands ¿ and the United Kingdom) and with the participation ¿ of ISAS and NASA.

2. Motivation

The original motivation for studying galaxy evolution in the infrared comes from our understanding of star formation within our own galaxy. In these regions the intrinsically bright optical and UV emission from young massive stars is strongly affected by dust. The effects of obscuration are less significant in the thermal infrared (1-3μm) and in the mid and far infrared we actually see the reprocessed emission from the dust. Thus to properly understand star-formation and hence galaxy formation we must study both optical and infrared wavelengths. Indeed actively star forming galaxies such as M82 emit significantly more power at far infrared wavelengths than in the optical and UV. The discovery that as much or more power in the extra-galactic background emerges at far-infrared/sub-mm wavelengths as in optical/UV bands [21], (see [22] for a review) emphasizes the cosmological importance of these far-infrared emitting populations. The unexpectedly numerous galaxies discovered by SCUBA (e.g. [23]) are expected to be star forming galaxies at high redshifts where the rest-frame far-infrared galaxies has been shifted to sub-mm wavelengths.

The ELAIS survey was designed to study the comparatively recent evolution of obscured star formation providing a bridge between local IRAS samples and SCUBA. It also aimed to understand the AGN phenomenon by exploring emission from the dusty tori.

3. Number Counts

The first evidence for galaxy evolution in any new survey inevitably comes from the number counts. We analysed the preliminary counts at 6.7, 15μm [8], 90μm [9] and the FIRBACK team presented the 175 μm counts [10]. The Final Analysis counts at 15μm in S1 and 90μm have been discussed by [24] and [13] respectively. Whichever wavelength you choose the result is the same: the counts are inconsistent with any no evolution predictions, i.e. we detect significant evolution at all wavelengths. This is illustrated at 15 and 90μm in Figure 1.

The departure from no evolution is particularly evident at 15 micron. In this band, the large dynamic range in flux density spanned by ELAIS (0.5-100 mJy), has allowed us to sample the source counts between the flat-Euclidean IRAS counts and the deep, ISOCAM counts ([25], [26], [27], [28], [29]). Moreover, the large area of the ELAIS survey means it provides a very precise measurement of the shape of the counts near 1-2 mJy, the critical flux density where the ISOCAM counts start diverging from no-evolution models.

The ability to detect strong evolution in sources down to $S \sim 0.5$ mJy within ELAIS has been possible thanks to the sophisticated reduction tools based on a

physical model of the detectors (Lari Method, [11]). These allowed us to observe at least a factor two deeper than expected.

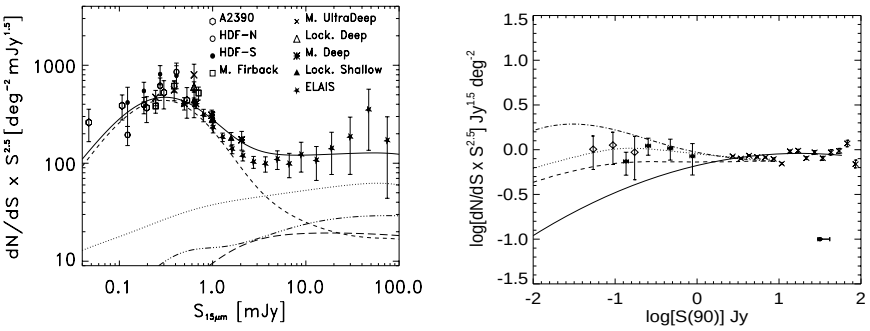

Figure 1. Number counts from ELAIS and other ISO surveys. Both show significant departures from no evolution models. Left: Differential–Euclidean normalised 15μm counts. Data points: ELAIS data from [24]; new A2390 data from [32] and new Lockman data from [34]. Other data points from [27]. Dashed, dotted, long-dashed and dot-dot-dot-dashed lines represent the model contribution for the spiral, the starburst, the Type-1 and the Type-2 AGN populations ([33],[38]). The solid line is the total. Adapted from [33].
Right: Differential–Euclidean normalised 90μm counts: ELAIS (solid symbol, [13]); Lockman Hole (open symbols, [35]) and IRAS PSC-z (crosses, [13]) compared with a no-evolution model (solid line). The dashed and dotted line represent model A and E from [36]. The dash-dotted line is the counts predicted by [37]. Taken from [13].

4. Multi-wavelength Identification

To investigate what sort of galaxies are responsible for the excessive numbers of galaxies seen at faint fluxes requires data at other wavelengths. There have been extensive observing imaging survey campaigns or comparisons with archival data at radio [18], [19], [39], optical [14], [15], [41], [42], [45], NIR [16], [17] and X-ray wavelengths [43], [44]. 80% have optical identifications to $R \sim 23$ [14] and 92% to $R \sim 24$ [15].

Redshifts have been obtained for 500 galaxies of our infrared samples (47% of the 15μm galaxies with identifications), primarily on AAT, ESO 3.6m, WHT, and other smaller telescopes. The median redshift distribution is 0.17 at 15 μm and 0.1 at 90 and 175 micron. In Figure 2 (right) we show the 15 μm redshift distribution, as summerised in [20]. Besides the strong peak around 0.2, a tail of sources at higher redshift, presumably the most luminous examples of the same sources which are seen in the deep surveys which have the redshift peak $z \sim 0.8$ ([29],[30],[31])

The optical spectra can be used to classify sources as AGN (Type-1 and Type-2), starburst galaxies and normal galaxies ([14]), [45]) About 75 % of the sources are starburst galaxies while $\sim$25% contain an AGN. About 20% of the galaxies show e(a) spectra [14] with both weak emission ($[OII]$) and absorption (H_δ). The e(a) galaxies are also found in the deep ISOCAM surveys ([46]) and are explained to be a result of selective dust extinction which affects the youngest, most massive, young stars in HII regions and they are believed to be associated with dust enshrouded starburst galaxies ([47]).

We have dissected the number counts in S1 using these classifications (Figure 2 (left), [14]). It is clear that the unidentified fraction increases as we go to fainter fluxes (where the excess over no evolution predictions becomes more extreme). Assuming that these unidentified sources are galaxies (as seen in deeper ISO surveys) rather than AGN then the galaxy fraction increases at fainter ISO fluxes. Overall we have an identified AGN fraction of around 25% [14].

The broad-band photometry from all the ISO instruments combined also provides a powerful constraint on the properties of the infrared emission processes. It appears that there are many luminous infrared galaxies with Arp220 like Spectral Energy Distributions (SEDs), but also, suprisingly, a large population of luminous $L_{\rm ir} > 10^{11.5} L_\odot$ galaxies with cool (cirrus-type) SEDs [20].

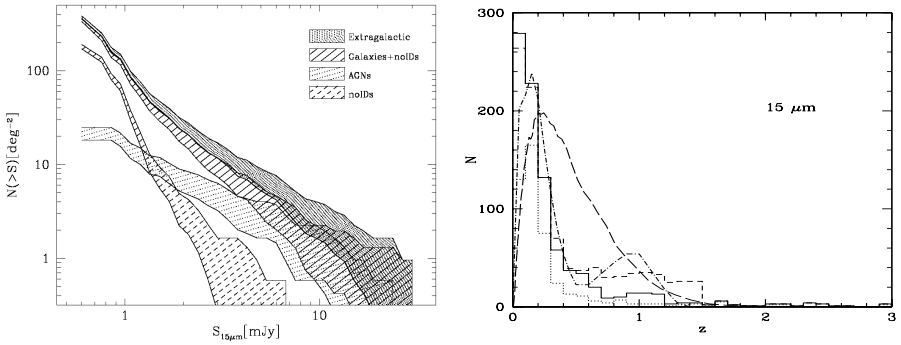

.

Figure 2. Left: Integral 15μm number counts from the ELAIS S1 field broken down by optical classes. Notice that the starburst/AGN fraction increases at fainter fluxes and, naturally, the unidentified fraction increases sharply at the faintest fluxes. (Taken from [14].) Right: Redshift distribution for ELAIS 15μm sources. Solid curve: both photometric and spectroscopic redshifts (840 sources), dotted curve: spectroscopic redshifts only (468 sources), broken curve: effect of assigning blank fields uniformly to range $0.5 < z < 1.5$. Long broken curve: predicted redshift distribution from [37], dash-dotted curve: predicted redshift distribution from [33]. Predictions take into account both the identified objects and the blank fields. Taken from [20]

5. Active Star-formation

As we have mentioned a significant fraction of the ELAIS sources have an Active Galactic Nuclei (AGN) [14]. It should be noted that the presence of an AGN does not necessarily mean the infrared luminosity is powered by the AGN. [20] model the infrared emission for all 306 galaxies with two or more IR bands and for only 34 (11%) does the AGN luminosity dominate. So a large fraction of the ELAIS sources are forming stars.

The optical photometry suggests a significant fraction of the sources have a high infrared to optical ratio and that this fraction increases as we move to fainter infrared fluxes and brighter infrared luminosities [14], [15] and [20]. The infrared/optical ratio is explore in Figure 3. Since the infrared luminosity is roughly proportional to star-formation rate and the optical is roughly proportional to stellar mass the ratio is some measure of the star-formation activity of efficiency in a galaxy. At low $L_{\rm FIR}$ this ratio is roughly constant, i.e. quiescent star formation, but at about $10^{10}L_{\odot}$, the ratio starts increasing and is fitted as $\log(L_{15}/L_R) = 0.47\log(L_{15}/L_{\odot}) - 5.02$ with a dispersion of 0.32 dex [14], where the total amount of star-formation is related to the strength of the "burst" which bears little correlation to the total stellar mass in the host galaxy (see e.g. Figure 3, right).

A number of galaxies show very high rates of activity $L_{\rm FIR}/L_{\rm Opt} \sim 100$ and very modest optical luminosities. Similarly [48] identify a population of extreme mid-to-near-IR objects (EMNOs), characterized by very high MIR/NIR flux ratios. However, they argue that their selection specifically picks out obscured AGN and nearly all appear to also be ULIRGs, and some are EROs.

In Figure 3, the 34 sources whose model infrared SED is dominated by an AGN are circled. As expected many of these fall in the optically luminous part of the diagram. Here there are other optically luminous sources which also presumably host AGN but which may not dominate the infrared luminosity. The infrared/optical ratio is less meaningful for any of these objects.

The importance of star-formation in these populations is also illustrated by the association between the 15μm sources and the 1.4GHz radio catalogues [39] which has revealed a mid-IR – radio correlation nearly as strong as the famous far infrared radio correlation (e.g. [49]). This correlation, shown in Figure 4, can be fitted as $\log(L_{1.4\rm GHz}/L_{\odot}) = (1.08 \pm 0.04\log(L_{15\mu\rm m}/L_{\odot}) - (6.07 \pm 0.41)$ with a dispersion of 0.27 dex (relation found taking into account also the radio upper limits). [39] also estimate the contribution of the infrared starbursts to the radio source counts and show that they are responsible for 60% of the counts at $S \lesssim 0.05$ mJy. ELAIS has been able to check the validity of the mid-IR – radio relation from the local Universe up to $z \sim 0.5$; deeper surveys have found that this relation is still valid up to $z \sim 0.8 - 1.0$ [40]. A statistical understanding of the star-forming populations and their evolution comes from studies of the

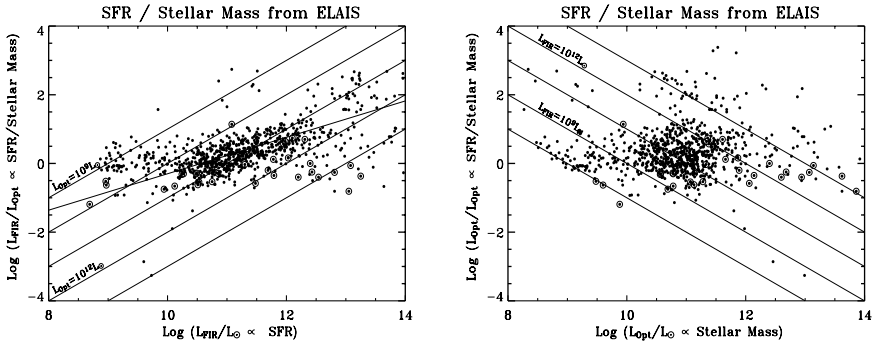

Figure 3. Left: Infrared excess vs IR correlation. Far-infrared luminosity estimated primarily from the 15μm band and optical, from *R*. Over-plotted are lines of constant optical luminosity and the fit reported by [14].
Right: The same information but plotted against $L_{\rm Opt}$ to better illustrate the poor correlation between activity and stellar mass at high star-formation rates. (Figures constructed from the final band-merged ELAIS catalogue, following [14], [20].)

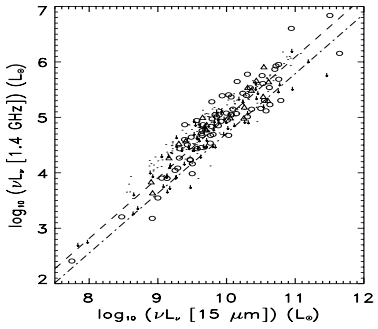

Figure 4. Mid-IR radio correlation. Dashed-line: best-fitting relation considering only radio detections; dot-dashed line: best-fitting relation considering also radio upper. Taken from [39].

luminosity functions. We have calculated the 15μm luminosity functions for galaxies [33]. The infrared to optical ratio was adopted as new criterion to separate the quiescent, non-evolving population from the rapidly evolving starbursts. For the starburst population, a combination of luminosity ($L \propto (1+z)^Q, Q \sim 3.5$) and density evolution ($\rho \propto (1+z)^P, P \sim 3.8$) provides the best fit, Figure 5 (left). This model, derived from the ELAIS data, also fits the full 15μm number counts (Figure 1, right) and the redshift distributions from the deeper ISOCAM surveys [29], [30], [31], [34]. We have also calculated the 90μm luminosity function from the Preliminary Analysis [51] and again from the Final Analysis

with more spectroscopic redshifts in [52], Figure 5 (right). This function is also significantly different from the redshift zero IRAS counterpart.

The ELAIS ISO data has also helped in the understanding of the star-forming galaxies seen by SCUBA. Using constraints on the SEDs of 19 $S_{850\mu m} > 8$mJy SCUBA sources [50] concluded that all had $z > 1$ and half had $z > 2$.

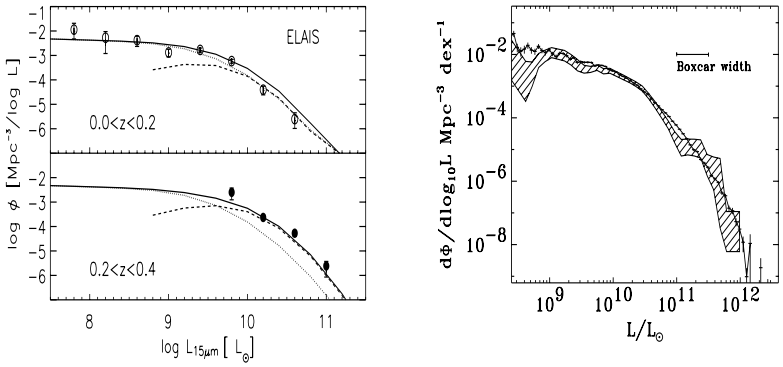

Figure 5. Left: Galaxy luminosity function at 15μm. Points represent the observed space density at different redshift, while lines represent the best-fit model predictions (dashed, dotted and solid lines: starburst, normal and starburst+ normal populations). Data split into $0 < z < 0.2$ and $z > 0.2$ intervals. Taken from [33]. Right: $z = 0$ luminosity function at 90μm from the ELAIS. The shaded area shows the $\pm 1\sigma$ estimate from the Final Analysis of the northern ELAIS fields. Pure luminosity evolution of $(1+z)^3$ is assumed. Luminosities are converted to bolometric luminosities assuming $\nu L_\nu =$constant. Also plotted is the predicted 90μm local luminosity function from the PSC-z survey [53]. Taken from [52].

6. Active Galactic Nuclei

As we have already said, SED modelling suggests around 11 percent of the infrared sources have SEDs dominated by emission from dusty tori around AGN. Also around 24% of the sources contain an AGN, even if it does not necessarily dominate the infrared luminosity. So it is clear that AGN are related, even if not causally, with the infrared galaxy phenomenon. It is interesting to note that the fraction of AGN seen in infrared galaxies increases with the infrared luminosity (Figure 6, left) an effect that had previously been noted in IRAS infrared galaxies at lower redshifts [54].

We have also calculated the 15μm luminosity functions for AGN (Type-1 and 2, [38], [55]). These show very significant evolution (see Figure 7). As yet

we have too few AGN to determine the luminosity function in different redshift bins, but the IRAS sample of [56] gives a low-z counterpart. The Type-1 AGN evolution is consistent with pure luminosity evolution at a rate of $(1+z)^Q$ with $Q \sim 2.6$, similar to that already seen for this type of sources at other wavelengths and the infrared galaxies. A similar evolution scenario is found for Type-2 AGN with $Q \sim 2-2.6$ (depending on the assumed SED) and this is the first time the shape and evolution for Type-2 AGN has been derived.

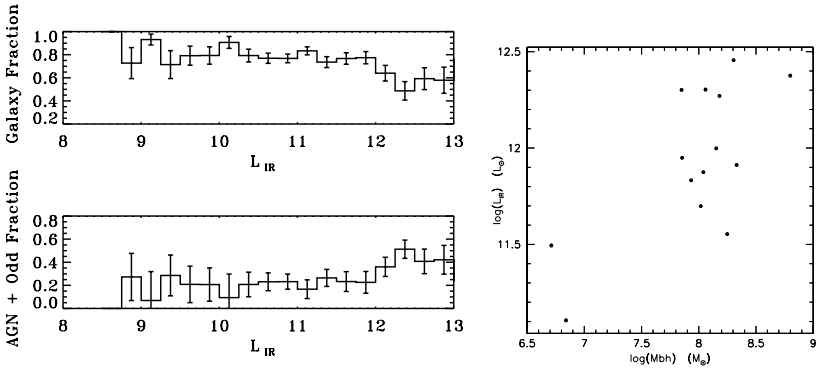

Figure 6. Left: Fraction of infrared galaxies containing (bottom, or *not* containing – top) an AGN as a function of infrared luminosity. Right: Infrared luminosity as a function of black hole mass, taken from [57].

[43] have investigated the 15 ELAIS sources that were also detected by ROSAT. 6 of these were broad-line QSOs, 4 were narrow-line star-forming galaxies or Type-2 AGN, 3 were stars, and 2 were unidentified optically. They did not find any particularly hard sources, arguing against heavily obscured AGN. [44] conducted a 2-10 keV survey over 2.5 square degree in S1 using Beppo-SAX. They found 17 hard X-ray sources, 10 of which had 15 μm counterparts and 8 of these have spectral classifications: 6 QSOs, 1 Type-2 AGN and one apparently normal galaxy. These observations were too faint to investigate the bulk of the ISO populations. [58] have investigated the associations between 15 μm sources and deep Chandra observations in ELAIS N1 and estimate an AGN fraction of 19% with the emission from the other ISO sources consistent with star-formation. A similar AGN fraction has been observed in deeper 15 micron fields using the same X/MIR correlation method (HDF-N and Lockman Hole: [59]). To-date, the X-ray surveys are either too small or too shallow to address this AGN fraction definitely.

[57] have investigated optically selected QSOs in the ELAIS N1 field and found that their optical properties are largely indistinguishable from the QSOs 15μm selected sample. They do find an apparent correlation between the black hole mass and the infrared luminosity (Figure 6, right).

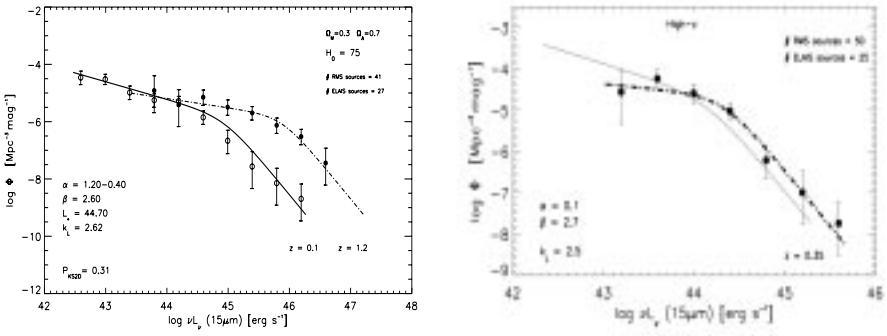

Figure 7. AGN luminosity functions at 15μm. Points represent the observed space density at different redshift, while lines represent the best-fit model predictions. Left: objects spectroscopically classified as Type-1 AGN; Right: objects spectroscopically classified as Type-2 AGN. The thin line represents the value of the fit at low-z ($z = 0.05$). Taken from [38].

7. Hyper-luminous galaxies

Objects as luminous as those seen in the SCUBA surveys are very rare. The wide areal coverage and large volume (5×10^6 Mpc^{-3}) of ELAIS makes it ideal for discovering rare objects such as these. So far we have discovered 9 galaxies whose infrared luminosities probably exceed $L > 10^{13.22} L_\odot$ [20] (60% of these are based on photometric redshifts and await spectroscopic confirmation). It is very likely that this number increases as the follow-up proceeds but this is already almost as many as have ever been discovered from the IRAS database. The bolometric emission from the first of these, ELAISP90 J1640101410502 [60], has been modeled with an almost equal contribution from star formation and accretion disk processes. Such objects may provide us with accessible "local" counterparts to the elusive SCUBA galaxies or, if they are unrelated, will provide interesting additional challenges to galaxy evolution models.

8. Large-scale structure

Very recently we have been able to analyse the clustering within ELAIS. In the southern field, S1, we have estimated the angular correlation function (Figure 8, [61]). Using the median redshift $z \sim 0.2$ [14] and inverting Limber's Equation we have estimated the 3D infrared galaxy-galaxy autocorrelation function with amplitude, encapsulated in the correlation length $r_0 = 4.3^{+1.0}_{-0.6}$ h^{-1}Mpc. This is consistent with measurements from local infrared samples ($r_0 = 3.79 \pm 0.14$ at $z \sim 0.02$, IRAS [65]; $r_0 = 3.7$ at $z \sim 0.02$, PSC-z [66]) and weaker than optical ($r_0 = 5.7$ at $z \sim 0.05$ – APM, [62]; $r_0 = 4.92 \pm 0.27$ at $z \sim 0.08$ – 2dFGRS, [64];

$r_0 = 5.7 \pm 0.2$ at $z \sim 0.18$ – SDSS, [63]). Our results thus conform to the existing picture i.e. the clustering strength of infrared samples is less than optically selected samples. This result appears to contradict that presented by [25] who found that in deep infrared surveys the infrared galaxies were more strongly clustered that the optical galaxies. However, this may suggest that within the ISO surveys we have already detected the evolution of clustering. Within the ELAIS survey itself [67] find a significant over-density of EROs around faint ELAIS mid-IR sources. A radial distribution of the EROs suggests a physical connection of these EROs and ISOCAM sources, which also suggests that the faintest ELAIS sources are more strongly clustered. This would be qualitatively consistent with the predictions of hierarchical models where star-formation occurs first in the strongly clustered peaks of the density field and takes longer to initiate in the lower density, more weakly clustered "field".

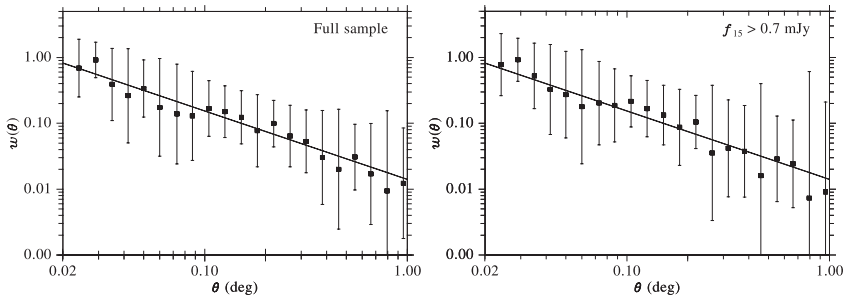

Figure 8. The Angular correlation function measured in our Southern field S1. Taken from [61]

9. The ELAIS Legacy

The ELAIS fields were carefully chosen to avoid contamination from dust emission from our own Galaxy [7]. Coupled with the ever expanding multi-wavelength data available the ELAIS fields are a prime target for new surveys. A number of surveys and projects have been carried out whose goals are relatively independent of the ISO observations themselves. Notable amongst these are the SCUBA 8mJy [71] and MAMBO surveys[72] and X-ray surveys [68], [69], [70]. These fields are particularly ideal for Spitzer and the ISO 15μm band data (inaccessible to Spitzer) will be extremely valuable. For example the GOODS validation field [75] was executed in ELAIS fields. More significantly, three of the ELAIS fields are core components of the SWIRE fields [73], [74].

10. Discussion

We have demonstrated that infrared emitting galaxies evolve strongly. The indications are that the star forming galaxies make up the bulk of the excess over no evolution predictions. Low star-formation rate (infrared luminosity) systems have similar infrared/optical ratios which is a measure of activity of the star-formation (star-formation rate per unit stellar mass) so their total star-formation rate is determined by the total stellar mass. However, at high star-formation rates there is a correlation between the infrared/optical excess and the infrared luminosity (total star-formation rate) and a corresponding lack of correlation with the optical luminosity (total stellar mass), indeed very high infrared/optical excess galaxies are found with very modest optical luminosities. This suggests that active star-formation is associated with factors external to the galaxy.

AGN are found in 20-25% of the sources, but star-formation may still be the dominant source of the infrared luminosity in all but 11% of the sources. The AGN and infrared phenomena are however, closely linked: the AGN fraction increases at higher IR luminosity; the infrared luminosity functions evolve at a similar rate; and the infrared luminosity is correlated to the black hole mass. This may imply a common factor in the AGN and star-formation phenomena.

At the extreme end we have discovered 9 hyper luminous galaxies, comparable with the total number discovered by IRAS.

We detect clustering with an amplitude consistent with lower redshift infrared samples and lower than optical samples, this contrasts with the higher clustering of infrared galaxies in a deeper sample suggesting that an evolution of clustering may have been detected in the ISO surveys.

It seems quite plausible that the environment provides the external factor determining active star-formation and the common factor linking star-formation and AGN activity, thus we might expect the evolution in the luminosity functions to be linked to an evolution in the clustering.

The ELAIS samples will provide invaluable templates for understanding the deeper samples detected by the Spitzer GTO and legacy surveys (e.g. [73], [76]) and the ELAIS fields themselves provide a valuable legacy for surveys with Spitzer and other facilities.

The complete ELAIS survey comprising a band-merged catalogue with multi-wavelength associations is now publicly available at the web address http://astro.imperial.ac.uk/Elais/

Acknowledgments

The authors would like to thank Michael Rowan-Robinson and the whole ELAIS team for their enormous efforts in making the ELAIS survey a reality and “we” in the text refers to the ELAIS team. We would like to thank Phillippe Héraudeau,

Israel Matute, Alejandro Afonso Luis and Evanthia Hatziminaoglou for providing figures in advance of publication and Petri Väisänen for useful comments. This chapter was based in part on an original conference proceeding [77].

References

1. M. Kessler, et al.: A&A, **315**, L27 (1996)
2. Kessler, M.F., Mller, T.G., Leech, K. et al. 2003, 'The ISO Handbook, Volume I: ISO - Mission & Satellite Overview', ESA SP–1262
3. C. Cesarsky, et al.: A&A, **315**, L32 (1996)
4. Blommaert, J., Siebenmorgen, R., Coulais, A. et al. 2003, 'The ISO Handbook, Volume II: CAM - The ISO Camera', ESA SP–1262
5. D. Lemke, et al.: A&A, **315**, L64 (1996)
6. Laureijs, R.J., Klaas, U., Richards, P.J. et al. 2003, 'The ISO Handbook, Volume IV: PHT - The Imaging Photo-Polarimeter', ESA SP–1262
7. S. Oliver, et al.: MNRAS **316**, 749 (2000)
8. S. Serjeant, et al.: MNRAS **316**, 768 (2000)
9. A. Efstathiou, et al.: MNRAS **319**, 1169 (2000)
10. H. Dole, et al.: A&A, **372**, 364 (2001)
11. C. Lari, et al.: MNRAS **325**,1173 (2001)
12. M. Vaccari, et al.: MNRAS submitted astro-ph/0404315 (2004)
13. P. Héraudeau, et al.: MNRAS, **354**, 924 (2004)
14. F. La Franca, et al.: AJ, **127**, 3075 (2004)
15. E. Gonzales-Solares, et al.: MNRAS, submitted, astro-ph/0402406 (2004)
16. P. Väisänen et al.: MNRAS **337**, 1043 (2002)
17. P. Väisänen , P. & P.H. Johansson: A&A, in press, astro-ph/0404129 (2004)
18. P. Ciliegi et al.: MNRAS **302**, 222 (1999)
19. C. Gruppioni et al.: MNRAS **305**, 297 (1999)
20. M. Rowan-Robinson, et al.: MNRAS, **351**, 1290 (2004)
21. J-L. Puget, et al.: A&A **308**, 5L (1996)
22. M.G. Hauser & E. Dwek: ARA&A, **39**, 249 (2001)
23. D. Hughes, et al.: Nature, **394**, 241 (1998)
24. C. Gruppioni, et al.: MNRAS, **335**, 831 (2002)
25. D. Elbaz, et al.: in Proceedings of 'Multiwavelength mapping of galaxy formation and evolution' conference held in Venice (Italy), October 2003, A. Renzini and R. Bender (Eds.) astro-ph/0403209 (2004)
26. S. Oliver, et al.: MNRAS, **289**, 471 (1997)
27. D. Elbaz, et al.: A&A, **351**, L37 (1999)
28. S. Oliver, et al.: MNRAS, **332**, 536 (2002)
29. H. Aussel, et al.: A&A, **342**, 313 (1999)
30. H. Flores, et al.: ApJ, **517**, 148 (1999)
31. H. Flores et al.: A&A, **415**, 885 (2004)
32. L. Metcalfe, et al.: A&A, **407**, 791 (2003)
33. F. Pozzi, et al.: ApJ, **609**, 122 (2004)
34. G.Rodighiero, et al.: A&A, **427**, 773 (2004)
35. G.Rodighiero, et al.: MNRAS, **419**, 55L (2004)
36. B. Guiderdoni et al.: MNRAS, **295**, 877 (1998)
37. M. Rowan-Robinson: ApJ **549**, 745 (2001)

38. I. Matute, et al.: in prep. (2004)
39. C. Gruppioni, et al.: MNRAS **341**, 1L (2003)
40. D. Elbaz et al.: A&A, **384**, 848 (2002)
41. R. G. McMahon, et al.: New Astronomy Reviews, **45**, Issue 1-2, 97 (2001)
42. T. Babbedge, et al.: MNRAS, **353**, 654 (2004)
43. D. Alexander, et al.: AJ **554**, 18 (2001)
44. S. Basilakos, et al.: MNRAS **331**, 417 (2002)
45. F. Pozzi, et al.: MNRAS, **343**, 1348 (2003)
46. H. Flores, et al.: ApJ, **517**, 148 (1999)
47. B. Poggianti & H. Wu: ApJ, **529**, 157 (2000)
48. P.H. Johansson, P. Väisänen, & M. Vaccari: A&A, **427**, 795 (2004)
49. J. Condon: ARA&A, **30**, 575 (1992)
50. M. Fox, et al.: MNRAS, **331**, 839 (2002)
51. S. Serjeant, et al.: MNRAS, **322**, 262 (2001)
52. S. Serjeant, et al.: MNRAS, MNRAS, **355**, 813 (2004)
53. S. Serjeant, & D. Harrison: Proceeding of the 'Multi-Wavelength Cosmology', Conference held in Mykonos, Greece, June 2003, ed. M. Plionis (Kluwer) (2004)
54. D.B Sanders & I.F. Mirabel: ARA&A, **34**, 749 (1996)
55. I. Matute, et al.: MNRAS, **332**, L11 (2002)
56. B. Rush, M.A. Malkan, L. Spinoglio L.: ApJS, **89**, 1 (1993)
57. A. Afonso-Luis et al.: MNRAS, **354**, 961 (2004)
58. J. Manners, et al.: MNRAS, **355**, 97 (2004)
59. D. Fadda D., et a.: A&A, **383**, 838 (2002)
60. T. Morel, et al.: MNRAS **327**, 1187 (2001)
61. E. Gonzales-Solares, et al.: MNRAS, **352**, 44 (2004)
62. S.J. Maddox, et al.: MNRAS, **242**, 43P (1990)
63. I. Zehavi, M. R. Blanton, J. A. Frieman, et al.: ApJ, **571**, 172 (2002)
64. P. Norberg, C. M. Baugh , E. Hawkins, et al.: MNRAS, **328**, 64 (2001)
65. W. Saunders, M. Rowan-Robinson & A. Lawrence: MNRAS, **258**, 134 (1992)
66. Y. P. Jing, G. Börner, & Y. Suto: ApJ, **564**, 15 (2002)
67. P. Vaisanen, & P.H. Johansson: A&A, in press, astro-ph/0405056 (2004)
68. C. Willott, et al.: MNRAS **339**, 297 (2003)
69. J. Manners, et al.: MNRAS **343**, 293 (2003)
70. C. Willott, et al.: ApJ **610**, 140 (2004)
71. S. Scott, et al.: MNRAS **331**, 817 (2002)
72. T. Greve, et al: MNRAS submitted astro-ph/0405361(2004)
73. C. Lonsdale, et al.: PASP, **115**, 897 (2003)
74. C. Lonsdale, et al.: ApJS, **154**, 54 (2004)
75. R. Chary, et al.: ApJS, ApJS, **154**, 80 (2004)
76. M. Dickinson, et al.: in Proceedings of 'Multiwavelength mapping of galaxy formation and evolution' conference held in Venice (Italy), October 2003, A. Renzini and R. Bender (Eds.) (2004)
77. S. Oliver, et al.: in Proceedings of 'Multiwavelength mapping of galaxy formation and evolution' conference held in Venice (Italy), October 2003, A. Renzini and R. Bender (Eds.) (2004)